Proceedings of the ASME 2011 5th International Conference on Energy Sustainability & 9th Fuel Cell Science,
Engineering and Technology Conference
ESFuelCell2011
August 7-10, 2011, Washington DC, USA

SAND2011-3710C

ESFuelCell2011-54159

THERMAL PROPERTY TESTING OF NITRATE THERMAL STORAGE SALTS IN THE SOLID-PHASE

Brian D. Iverson
Sandia National Laboratories
Albuquerque, NM, USA

Joseph G. Cordaro
Sandia National Laboratories
Livermore, CA, USA

Alan M. Kruizenga
Sandia National Laboratories
Livermore, CA, USA

ABSTRACT

Implementation of molten salt compounds as the heat transfer fluid and energy storage medium provides specific benefits to energy collection and conversion. Nitrate salts have been identified as a strong candidate for energy transfer and storage and have been demonstrated for use in these applications over time. As nitrate salts have solidification temperatures above ambient, concern for recovery from salt freezing events has instigated efforts to understand and predict this behavior. Accurate information of salt property behavior in the solid-phase is necessary for understanding recovery from a freeze event as well as for phase change thermal energy storage applications. Thermal properties for three representative salts (that span the range of melting temperatures from approximately 90 – 221 °C), have been obtained. These properties include specific heat, coefficient of thermal expansion, and thermal conductivity. Specific heat and thermal conductivity were measured using differential scanning calorimetry.

INTRODUCTION

Interest in raising the operating temperature of concentrating solar technologies and the incorporation of thermal storage has motivated studies on the implementation of molten salt as the system working fluid. Recently, salt has been considered for use in trough-based solar collectors and has been shown to offer a reduction in levelized cost of energy as well as increased availability [1]. Concerns regarding the use of molten salt in troughs are often related to issues with salt solidification and recovery from freeze events. Differences among salts used for heat transfer and storage are typically designated by a comparison of liquid phase thermal properties and cost. However, the potential for a freeze event necessitates an understanding of salt thermal and mechanical properties in the solid-phase in order to characterize and mitigate possible detrimental effects during freeze event recovery. This includes stress imparted by the expanding salt. Initial modeling efforts of tube stress during freeze event recovery have been reported [2].

Additionally, significant attention has been given to using salts as a phase change storage media (using encapsulation and otherwise). Property changes as a function of temperature as well as an understanding of solid-phase behavior are critical in characterizing systems of this type. Salt volumetric changes and thermal transport are paramount in storage applications.

For freeze event recovery and phase change thermal energy storage, reliable material property data are an integral part to model validation. Previous modeling efforts have assumed mechanical properties similar to published data on common salts. In this work, data is presented for measured thermal properties of three salts used for heat transfer and storage. Samples of solar salt, HITEC salt (Coastal Chemical Co.) and a low melting point quaternary salt (developed at Sandia National Laboratories) were cast for solid-phase characterization tests to determine specific heat, coefficient of thermal expansion (CTE), and thermal conductivity. The quaternary salt is a newer formulation that has been studied from a material behavior standpoint but has not been applied in a solar field to date. Where possible, experiments were conducted over a range of temperatures below the melting point to measure temperature-dependency of some physical properties in the solid-phase. This work is presented as an extension to the temperature dependent mechanical properties (unconfined compressive strength, indirect tensile strength, Young's modulus, and Poisson's ratio), previously reported [3].

In an effort to span the typical range of melting point possibilities of thermal storage salts, three representative salts were selected for property testing: solar salt (60 wt% $NaNO_3$, 40 wt% KNO_3)[4, 5], HITEC salt (40 wt% $NaNO_2$, 7 wt% $NaNO_3$, 53 wt% KNO_3)[6], and a low melting point quaternary salt (42.3 wt% KNO_3, 39.4 wt% $Ca(NO_3)_2$, 12.1 wt% NaNO3, 6.1 wt% LiNO3)[7]. For simplicity the solar, HITEC and quaternary salts are referred to as salts A, B, and C, respectively. Table 1 lists the melting temperature (T_m) for each case along with a summary of the temperature ranges over which the tests were performed.

Table 1. Approximate temperature ranges and melting temperatures for thermal property testing of each material.

Salt Type	Specific heat	CTE	Thermal conductivity
Solar salt [4, 5] $T_{m,A}$ = 221 °C	0 to 325 °C	30 to 200 °C	30 to 35 °C
HITEC [6] $T_{m,B}$ = 142 °C	0 to 250 °C	30 to 120 °C	30 to 35 °C
Quaternary [7] $T_{m,C}$ = 90 °C	-50 to 250 °C	30 to 75 °C	n/a

SPECIFIC HEAT

Sample Preparation and Test Procedure

Cylindrical pieces of each salt were cast in a PTFE tube with silicone stopper and extracted for property testing. The samples were cooled at room temperature. Sample sizes of roughly 100 mg were sectioned for specific heat measurement.

A form of temperature-modulated differential scanning calorimetry (TMDSC) was employed to measure specific heat of salt samples (Mettler Toledo DSC 823). The samples were subjected to a linear temperature-increase rate with a superimposed stochastic modulated temperature fluctuation. Based on the frequency response of the heat flow profile, the heat capacity can be obtained from the sample. Information on this method can be found in various references [12, 13] and in many respects is similar to ASTM standard E1269. However, the temperature-modulated approach (TOPEM) allows for direct measurement of the specific heat capacity instead of requiring an indirect comparison with a standard material. Further, using random temperature modulations, the heat capacity can be determined over a broad frequency range from one single measurement.

For each salt, the sample temperature was increased from a temperature at or below room temperature up to at least 100 °C above the melt temperature. Testing over a broad range of temperatures in this manner, allowed us to capture the specific heat observed throughout the solid phase and provide an indication of the specific heat in the liquid phase at low temperatures for comparison.

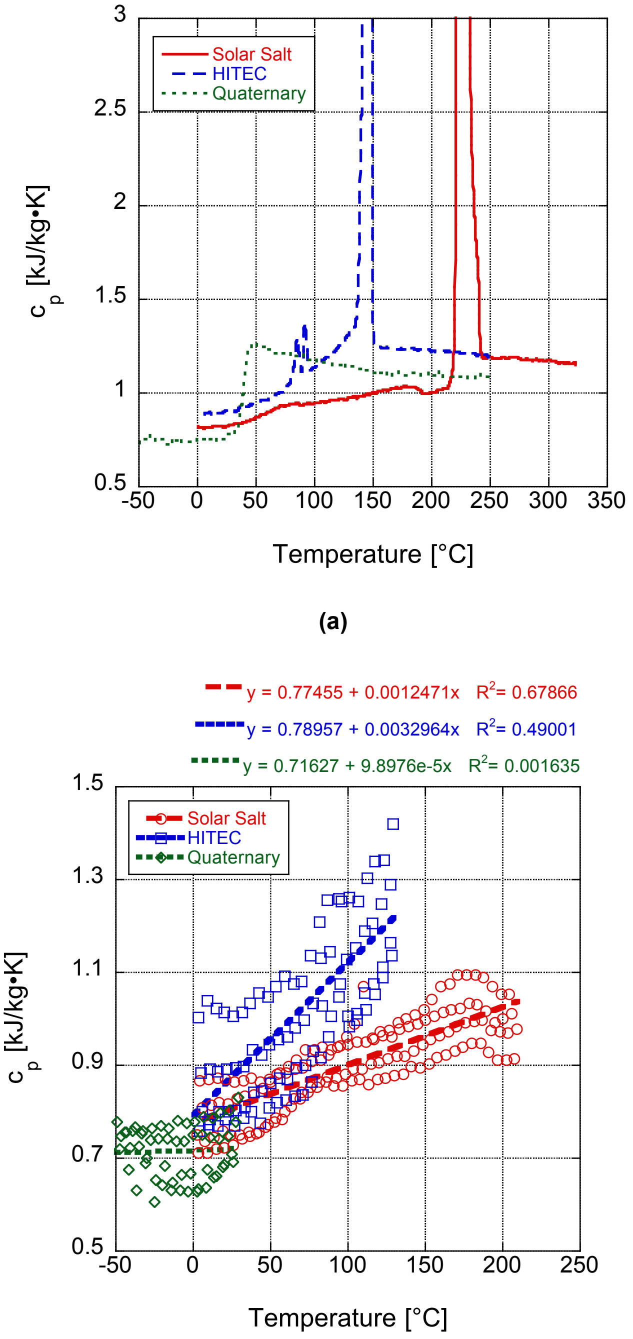

(a)

(b)

Figure 1. Solid-phase specific heat as a function of temperature for solar, HITEC and quaternary salts through (a) 100 °C above melt and (b) just below the onset of melting.

Test Results

Specific heat values as a function of temperature obtained using differential scanning calorimetry (DSC) are presented in Figure 1. Values were obtained from 0 °C through 100 °C above the melt temperature for each salt. The measurement was repeated four times with nearly identical results. A sample curve for each salt was selected and plotted in Figure 1a. The strong peak observed in solar and HITEC salt indicates the phase change process from solid to liquid. A slight increase is observed in the solid-phase specific heat with temperature whereas a flat profile is observed in the liquid-phase for the temperature ranges considered.

Figure 1b illustrates specific heat values in the solid phase only (up to about 10 °C below the melt temperature for solar and HITEC salts). Data points from repeat measurements were included and a linear regression performed to indicate temperature dependence. The values for HITEC agree well with the single reported value of 1.34 kJ/kg·K (no specific temperature provided) [6]. The quaternary salt exhibits a very flat profile in the solid phase up to about room temperature. However, in Figure 1a, a marked increase in c_p is observed below 50 °C, well below the melt temperature of 90 °C. In fact, this material exhibits a glasslike specific heat transition from solid to liquid without a large spike as observed in solar and HITEC salts. It is possible that there are solid-solid phase transitions occurring at these temperatures below the melt and is likely impacted by the fact that it is off-eutectic. For this reason, the quaternary salt data points presented in Figure 1b, and used to calculated the solid-phase c_p, only include temperatures up to ~30 °C.

Figure 2 illustrates the melting process for the three salts (arranged in each picture in the following order: quaternary, HITEC and solar salt). Each image is at a different temperature with light-colored regions indicating opacity due to the presence of solid-phase components. At temperatures below the melt temperature of 90 °C, the quaternary salt exhibits phase transitions with glass-like behavior, indicative of early melting.

Table 2. Specific heat values at specified temperatures for solar salt, HITEC and quaternary salts. Values in the solid phase were obtained from the linear regression equations in Figure 1b; liquid values were obtained from an average of four repeat measurements at the specified temperatures.

		c_p [kJ/kg·K] (standard deviation)		
Temperature	Phase	Solar Salt	HITEC	Quaternary
25 °C	solid	0.81 (0.07)	0.87 (0.11)	0.72 (0.06)
$T_m - 10$ °C	solid	1.04 (0.06)	1.22 (0.14)	n/a
$T_m + 50$ °C	liquid	1.11 (0.08)	1.17 (0.11)	1.15 (0.07)

Values for specific heat at 25 °C, 10 °C below the melt temperature and 50 °C above the melt temperature for each salt is provided in Table 2. The standard deviation of the data points at a given temperature divided by the average c_p at that temperature for each salt illustrates that the expected scatter in measurement is less than 15% of the average value in the solid-phase.

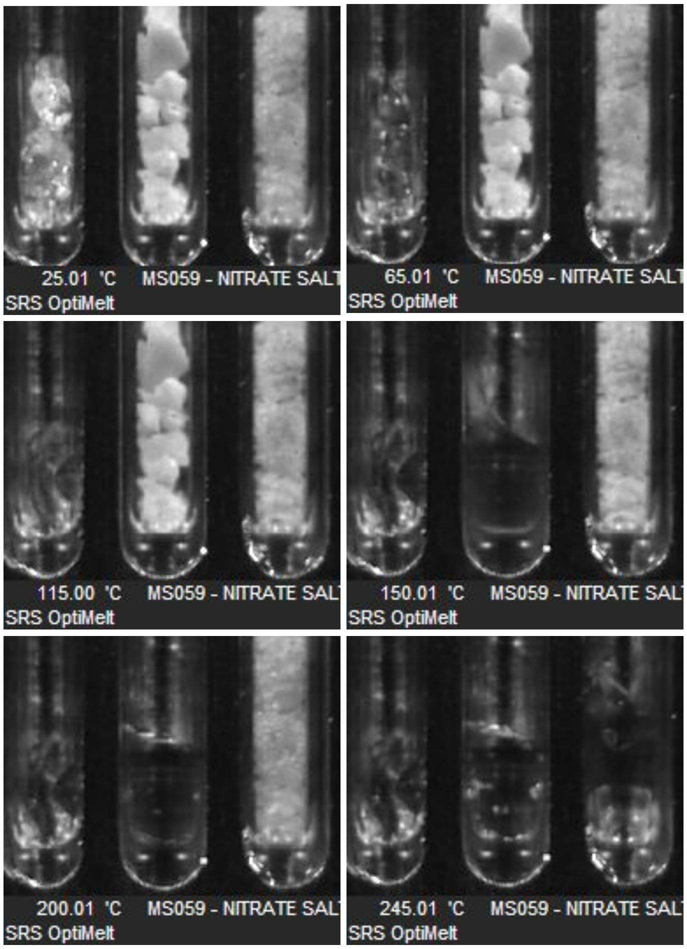

Figure 2. Images illustrating light intensity passing through the salts (in order from left to right of increasing melt temperature, i.e., quaternary, HITEC, and solar salt) for six temperatures ranging from room temperature to 245 °C. Lighter colors indicate less light passage due to the presence of the solid-phase.

COEFFICIENT OF THERMAL EXPANSION

Sample Preparation

Cylindrical samples (with diameter of approximately 5.08 cm and cut to length) were cast in a PTFE tube with silicone stopper and extracted for property testing. Molten salt was poured so as to fill the PTFE tube contiguously and avoid layer formation in the salt. The samples were cooled at room temperature. Cratering near the top of the samples (due to phase-dependent density change) and void formation in the salt-core interior were avoided by cross sectioning and identifying unaffected regions of the solidified salt. Solar salt, which has a large volume increase during phase change from solid to liquid (4.6%), had the most pronounced cratering [4, 5]. The quaternary salt had no visible cratering.

All CTE samples of were cut using a wire saw to nominally 4.7 cm in length. Solar salt and HITEC samples were turned on a lathe to 2.3 cm in diameter. Quaternary salt samples proved to be very difficult to machine given their glasslike behavior; therefore, samples were cast to a diameter of 1.5 cm before being cut to length. The estimated porosity is less than about 5% for all salt types, as computed from the measured dimensional density divided by the sum of the constituent theoretical densities. Two polycrystalline samples of each salt material with undetermined grain size were sent to Harrop Industries, Inc. for CTE measurement.

Test Procedure and Results

Salt samples were loaded into a temperature controlled oven with a long push rod and heated at 3 °C/minute. Each sample was heated and then cooled back to its starting temperature. The target high temperature was approximately 90% of the melting temperature. Expansion and contraction of the salt was recorded using linear displacement transducers relative to the starting point throughout the test procedure. The test procedure follows ASTM E228.

Figure 3 and 4 illustrate the percent elongation (relative to the initial length at room temperature) as a function of temperature for all three salt types. A repeat experiment was performed for each salt type yielding similar results; values for all CTE experiments are provided in Table 3. Solid lines in Figure 3 and 4 represent actual data collected (at 0.1-0.2 °C increments) while the dashed and dotted lines represent the least-squares best fit (linear regression) over the heating and cooling regions. The slopes of these curve fits correspond with the best-fit values in Table 3. Averages of the two test samples for each material over the heating and cooling regions are provided in the "Avg" column of Table 3. For samples of solar salt and HITEC, there appears to be continued expansion of the materials when the temperature is said to be decreasing. This effect may indicate that there was some thermal inertia coupled with the heating and cooling rate for the selected sample size that was slightly high and resulted in a possible non-uniform temperature throughout the sample. The values of CTE for solar salt and HITEC are similar for both heating and cooling (Table 3). Both salts exhibit rather linear thermal expansion upon heating and both expand slightly for the first 10-20 °C of cooling. A single reported value for the thermal expansion of solid-phase HITEC salt has been reported as 51.3 x 10^{-6} °C^{-1} [6]. This value agrees well with the CTE values measured upon heating (see Table 3).

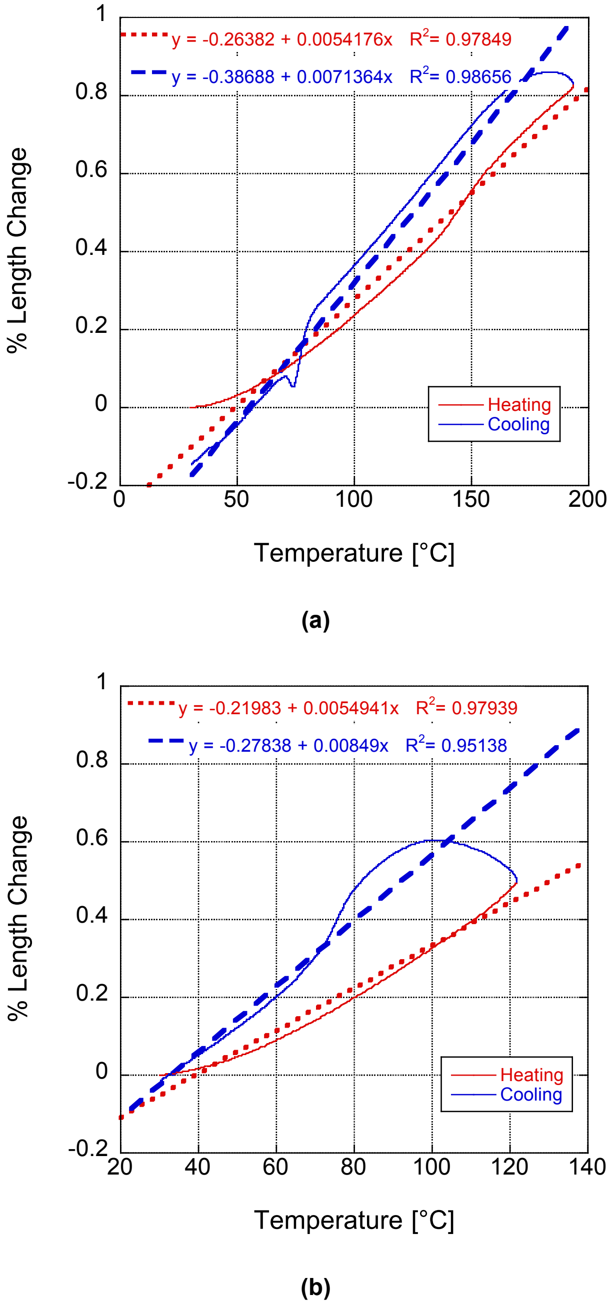

(a)

(b)

Figure 3. Percent length change as a function of temperature for (a) solar salt sample 1A, (b) HITEC salt sample 3B. Data points are taken at 0.1-0.2 °C increments with error values of <0.05% in length change and ±1 °C in temperature. Trend lines are generated using all data points from the heating or cooling regions.

For the purpose of comparison, the CTE of Halite (NaCl) is presented at the bottom of Table 3. The first value of 40 × 10^{-6} °C^{-1} was selected at a temperature near the midrange (~75 °C) of test temperatures for solar salt and HITEC [8]. The second value given for Halite of 45.0 × 10^{-6} °C^{-1} was defined as the coefficient of linear thermal expansion and therefore implies temperature independence [9]. CTE for solar salt and HITEC are more than 30% higher than that for naturally occurring polycrystalline Halite. As an additional comparison, the coefficient of thermal expansion for steels ranges from 10-20 × 10^{-6} °C^{-1} [10].

Table 3. Coefficient of thermal expansion values over specified ranges.

Salt type	Sample	Heat/cool range [°C]	α / 10^{-6} °C^{-1}	
			Best fit	Avg
Solar salt	1A	Heat 30.1 – 193.3	54.2	Heat
		Cool 193.3 – 30.4	71.4	54.7
	2A	Heat 30.0 – 199.2	55.2	Cool
		Cool 199.2 – 30.4	69.8	70.6
HITEC	3B	Heat 30.0 – 121.6	54.9	Heat
		Cool 121.6 – 30.4	84.9	55.8
	4B	Heat 30.0 – 120.2	56.7	Cool
		Cool 120.2 – 30.4	83.7	84.3
Quaternary	5C	Heat 28.0 – 42.0	46.2	Heat
		Cool 42.0 – 28.5	33.6	56.4
	6C	Heat 25.0 – 42.0	66.5	Cool
		Cool 42.0 – 35.7	24.8	29.2
Halite (NaCl)	N/A	Heat (~75 °C)	~ 40 [8]	
		unknown	45.0 [9]	

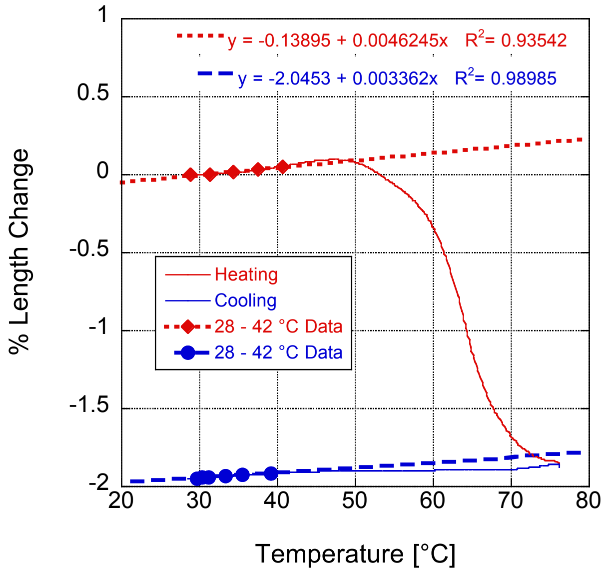

Figure 4. Percent length change as a function of temperature for quaternary salt sample 5C. Data points are taken at 0.1-0.2 °C increments with error values of <0.05% in length change and ±1 °C in temperature. Trend lines are based on the data points collected only for the temperature range from 28.0-42.0 °C for heating and 28.5-42.0 °C for cooling as indicated by selected data points on the figure.

The behavior of the quaternary salt (Figure 4) is markedly different from that for solar salt and HITEC (Figure 3). A small length change was observed upon heating to about 50 °C. From 50 °C to 90% of the melt temperature, the quaternary salt exhibited contraction. The pressure applied on the sample during measurement was calculated to be 8.48 MPa. Although small, this non-zero pressure is likely linked to the observed shrinkage. It is possible that the low melting point of the quaternary salt coupled with the fact this non-eutectic salt exhibits glasslike behavior may have caused the measurement probe to sink into the sample at temperatures below the melt temperature. However, Figure 4 indicates there is a somewhat linear region from 28-42 °C for both the heating and cooling cycles. Calculating the CTE within this region may more accurately represent the material behavior. The temperature ranges and best-fit values listed in Table 3 are based on this limited range. For the starting temperature up to 42 °C and from 42 °C down to room temperature, the CTE of the quaternary salt averages 56.4 × 10^{-6} °C^{-1} and 29.2 × 10^{-6} °C^{-1}, respectively.

THERMAL CONDUCTIVITY

Sample Preparation

Similar to the CTE samples, cylindrical pieces of each salt were cast in a PTFE tube with silicone stopper and extracted for property testing. Molten salt was poured so as to fill the PTFE tube contiguously and avoid layer formation in the salt. The samples were cooled at room temperature. Cratering was again avoided by cross sectioning and identifying unaffected regions. Initial cutting of all CTE samples was performed using a lathe and wire saw to achieve a prescribed diameter (5.84 mm) and then cut to small segments a few mm in length. These segments were then sanded to achieve thickness of 1.5-3.0 mm. Special care was taken to ensure that the sides of small disks were perpendicular to the flat ends of the cylinder. Owing to the glasslike nature of the quaternary salt, machining parts to a diameter of 5.84 mm was problematic. This precluded the quaternary salts from being evaluated using the methods employed here for thermal conductivity.

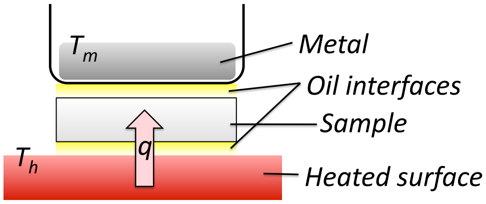

Figure 5. Test configuration for thermal conductivity using DSC.

Test Procedure

Following a procedure established by Riesen [11], DSC was used to establish heat flow through a sample salt disk to a crucible containing the low melting point metal gallium (T_m = 29.76 °C, see Figure 5). Interfaces between the salt disk, heated surface and crucible were filled with a small amount heat transfer oil to maintain reproducibility.

The total resistance to heat flow through this stack is the proportionality constant between the thermal power (q) and temperature difference (ΔT). For the oil interface resistances (R_{int}) and sample resistance (R_s) between the metal and heated surface, we obtain

$$q = \frac{\Delta T}{\Sigma R} = \frac{T_h - T_m}{R_{int} + R_s + R_{int}}. \tag{1}$$

The melt temperature of the metal (T_m) is known and the heated surface temperature (T_h) and q are obtained during the DSC measurement. The resistance due to the oil at both interfaces and across samples can be assumed to be the same since the same sample cross section is used. Thus, we define

$$R_{t,int} = R_{int} + R_{int}\ . \tag{2}$$

The total interface resistance ($R_{t,int}$) can be determined by performing multiple measurements on similar samples. If $R_{t,int} << R_s$, then $R_{t,int}$ can be neglected.

Assuming a small $R_{t,int}$, one-dimensional heat flow, steady state, and no internal generation, the heat flow is defined by

$$q = \frac{L}{kA}\left(T_h - T_m\right) \tag{3}$$

where L is the thickness of the sample, k is the sample thermal conductivity, and A is the cross sectional area. Equation 3 can be solved for the conductivity of the material directly from a single melting curve, assuming $R_{t,int}$ is small. When $R_{t,int}$ is not negligible, we can define the slope of the linear side of the melting peak (see also Figure 6a) as

$$S = \frac{q(t) - q_{onset}}{T_h(t) - T_{onset}} = \frac{1}{R_{t,int} + L/kA} \tag{4}$$

where q_{onset} and T_{onset} are the heat flow and melt temperature of metal at the onset of melting. When two samples of the same material and different thicknesses are measured, the thermal conductivity of the sample can be obtained by

$$k = \frac{\Delta L}{A\left(\frac{1}{S_2} - \frac{1}{S_1}\right)}. \tag{5}$$

When several samples of different heights are used, the thermal conductivity and $R_{t,int}$ can be determined by rearranging equation 4 and using a linear regression to obtain k, as follows

$$\frac{1}{S} = \frac{L}{kA} + R_{t,int}\ . \tag{6}$$

Test Results

As a validation of the procedure outlined for thermal conductivity above, measurements were made on PTFE and compared to literature values and previous DSC based measurements. Using a direct approach following equation 3 (neglecting interface resistance) and averaging over the linear range of the heat flow vs. temperature curve, we obtained a thermal conductivity value of 0.206 W/m·K for PTFE (error of 17.6%). By using the linear regression approach following equation 6 on multiple measurements of PTFE with varying thicknesses, we obtained 0.247 W/m·K (error of 1.2%). These value agree well with an accepted literature value of 0.25 W/m·K and is an improvement over the 0.181 W/mK measurement reported in Mettler Toledo's UserCom [11] thus lending confidence to the measurement technique.

Figure 6a illustrates an example heat flow curve as a function of temperature for a solar salt sample of thickness 2.5 mm. Here the onset of melting of the metal (Figure 5) is observed at approximately 30.5 °C. The linear portion of this curve, immediately following the onset of melt is used to determine the slope parameter, S (equation 4), for each measurement taken. The inverse of this slope from the linear region of each sample is then plotted as a function of the geometric ratio L/A as in Figure 6b and Figure 7. Samples were prepared in four thicknesses; multiple stacked samples provided the upper range of material thicknesses as indicated in the figures. Thermal conductivity is obtained in two ways from the data in these figures. First, thermal conductivity was measured directly (k_{direct}) following equation 3 and averaged over all samples. Second, a linear regression was performed to represent the measurement data of Figure 6b and Figure 7 where the inverse of the slope of the regression model yields thermal conductivity of the material ($k_{regression}$). Thermal conductivity values obtained in these fashions are listed in Table 4 along with standard deviation and R^2 values to indicate variability.

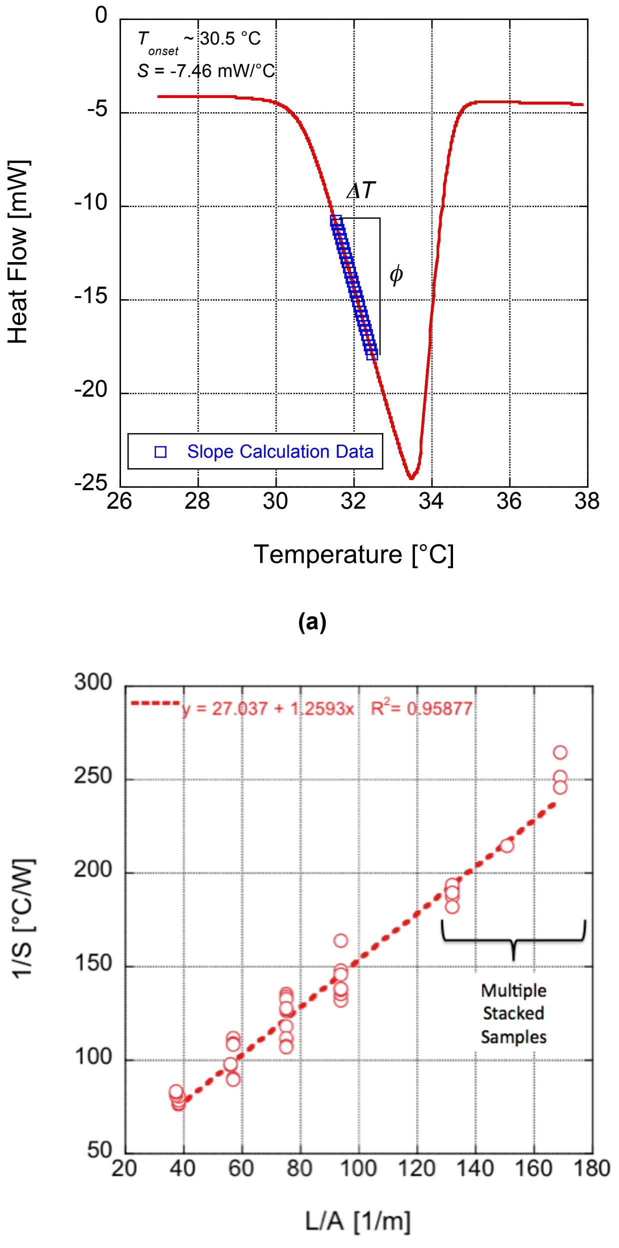

(a)

(b)

Figure 6. (a) Example heat flow vs. temperature curve for solar salt sample of thickness 2.5 mm. (b) Measurement data for solar salt samples of 4 different thicknesses and a combination of multiple stacked samples following equation 6. The inverse of the slope of the linear regression trend line yields the regression-based thermal conductivity of the material.

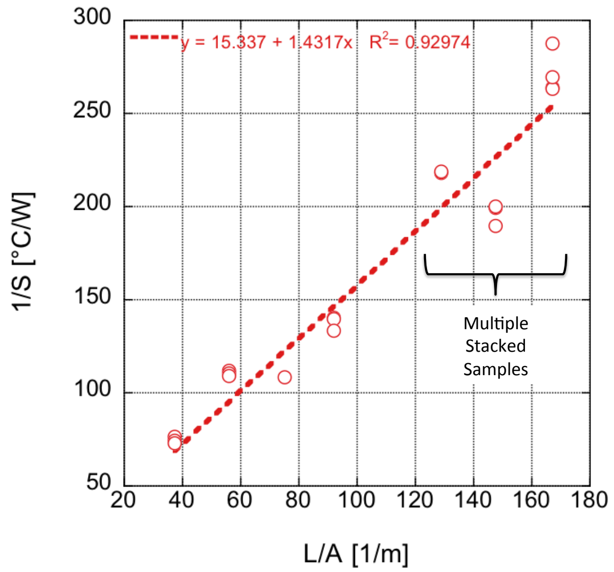

Figure 7. Measured data for HITEC samples of 4 different thicknesses and a combination of multiple stacked samples following equation 6. The inverse of the slope of the linear regression trend line yields the regression-based thermal conductivity of the material.

Although made of different compositions, solar salt and HITEC demonstrate similar thermal conductivity values. Previous reporting indicates that the thermal conductivity of HITEC in the liquid phase appears to approach 0.44 W/m·K as the temperature decreases towards solidification [6]. However, information below solidification temperature has not been presented previously.

Table 4. Measured thermal conductivity for solar salt and HITEC using direct and linear regression approaches.

	Solar Salt	HITEC
k_{direct} [W/m·K]	0.76	0.74
Standard deviation	0.12	0.10
$k_{regression}$ [W/m·K]	0.79	0.70
R^2 value of regression	0.96	0.93

CONCLUSIONS

Thermal properties of three representative salts for use in thermal storage systems have been evaluated. The nitrate salts (solar, HITEC, and quaternary salts) span a wide range of melting temperatures from 90 – 221 °C. Measured values for coefficient of thermal expansion were obtained using linear displacement transducers with samples temperatures ramped to approximately 90% of the melting temperature. Thermal conductivity and specific heat were obtained using multiple DSC techniques. Thermal property values in the solid-phase enable modeling of freeze recovery strategies and phase change storage when combined with previously reported mechanical property data.

ACKNOWLEDGMENTS

This manuscript has been authored by Sandia Corporation, a Lockheed Martin Company, under Contract No. DE-AC04-94AL85000 with the U.S. Department of Energy.

REFERENCES

[1] Kearney, D., Herrmann, U., Nava, P., Kelly, B., Mahoney, R., Pacheco, J., Cable, R., Potrovitza, N., Blake, D., and Price, H., 2003, "Assessment of a molten salt heat transfer fluid in a parabolic trough solar field," *Journal of Solar Energy Engineering*, Vol. 125, pp. 170-176.

[2] Kolb, G. J., Ho, C., Iverson, B. D., Moss, T. A., and Siegel, N. P., 2010, "Freeze-thaw tests of trough receivers employing a molten salt working fluid," ASME Energy Sustainability, May 17-22, 2010, Phoenix, AZ, USA.

[3] Iverson, B. D., Broome, S. T., and Siegel, N. P., 2010, "Temperature dependent mechanical property testing of nitrate thermal storage salts," SolarPACES, September 21-24, 2010, Perpignan, France.

[4] Pacheco, J. E., Ralph, M. E., Chavez, J. M., Dunkin, S. R., Rush, E. E., Ghanbari, C. M., and Matthews, M. W., 1994, "Results of molten salt panel and component experiments for solar central receivers: cold fill, freeze/thaw, thermal cycling and shock, and instrumentation tests," SAND94-2525, Sandia National Laboratories.

[5] Bradshaw, R. W. and Carling, R. W., 1987, "A review of the chemical and physical properties of molten alkali nitrate salts and their effects on materials used for solar central receivers," SAND87-8005, Sandia National Laboratories.

[6] Coastal Chemical Company, "HITEC Heat Transfer Salt," accessed April 19, 2010 from http://www.coastalchem.com/process-literature-files.html.

[7] Bradshaw, R. W., Cordaro, J. G., and Siegel, N. P., 2009, "Molten nitrate salt development for thermal energy storage in parabolic trough solar power systems," ASME Energy Sustainability, July 19-23, 2009, San Francisco, CA.

[8] Drebushchak, V. A. and Turkin, A. I., 2001, "Relationship between heat capacity and thermal expansion derived from the Lennard-Jones potential," *Journal of Thermal Analysis and Calorimetry*, Vol. 65, pp. 745-753.

[9] Callahan, G. D. and DeVries, K. L., 1994, "WIPP benchmark calculations with the large strain SPECTROM codes," SAND94-1376, Sandia National Laboratories, Albuquerque, NM.

[10] MatWeb, 2011, "Material property data," accessed May 3, 2011 from http://www.matweb.com.

[11] Riesen, R., 2005, "Simple determination of the thermal conductivity of polymers by DSC," UserCom 22, 2/2005, Mettler-Toledo, pp. 19-23.

[12] Schawe, J., 2005, "The separation of sensible and latent heat flow using TOPEM®," UserCom 22, 2/2005, Mettler-Toledo, pp. 16-19.

[13] Schawe, J. E. K., Hutter, T., Heitz, C., Alig, I., and Lellinger, D., 2006, "Stochastic temperature modulation: A new techniqe in temperature-modulated DSC," *Thermochimica Acta*, Vol. 446, pp. 147-155.